EQA - International Journal of Environmental Quality
ISSN 2281-4485 - Vol. 61 (2024): 1-15
Journal homepage: https://eqa.unibo.it/

published by

The adsorption of Pb^{2+} and Ni^{2+} ions utilizing modified chitosan beads: A response surface methodology and artificial neural network modelling study

Ephraim Igberase*, Nastassia Thandiwe Sithole

University of Johannesburg, Department of Chemical Engineering, Doornfontein, South Africa

* Corresponding author E-mail: ephraimigberase@gmail.com

Article info
Received 16/11/2023; received in revised form 4/4/2024; accepted 20/4/2024 DOI: 10.6092/issn.2281-4485/18471

The article has been retracted, see the retraction notice: https://doi.org/10.6092/issn.2281-4485/20311.

Abstract
This work investigates the application of artificial neural networks (ANN) and response surface methodology (RSM) in developing a technique for removing Pb^{2+} and Ni^{2+} ions from wastewater using chitosan derivative. The materials including chitosan beads (CS) and grafted chitosan beads (MCS) were evaluated using infrared spectroscopy (FTIR) and a scanning electron microscope (SEM). The process factors were modeled and optimized using the central composite design (CCD) derived from RSM. Removal efficiency was described as the response for the output layer. However, the input layer feed data consists of pH, adsorbent dose, contact duration, temperature, and concentration. Two neurons were used as the ANN algorithm's output layers, which correspond to the adsorption of Pb^{2+} and Ni^{2+} ions. Both models were measured using statistical metrics like average relative errors (ARE), coefficient of determination (R^2), Marquart's percentage standard deviation (MPSD), mean squared error (MSE), Pearson's Chi-square (χ^2), root means square errors (RMSE), and the sum of squares of errors (SSE). The ideal trained neural network depicts the training, validation, and testing phases, with R^2 values of 1.0, 0.968, and 0.961, respectively. The findings, however, showed that the ANN technique is superior to the RSM-CCD model approach. At pH 5, starting concentration of 100 mg/L, an adsorbent mass of 6.0 g, a reaction time of 55 min, and a temperature of 40 °C, the RSM-CCD model's optimization results for the process variables were achieved. The greatest removal percentages for Pb^{2+} and Ni^{2+} ion was 98.14% and 98.12%, respectively. The findings suggest that ANN can be utilized in forecasting the removal of adsorbates from wastewater.

Keywords
Adsorption, Response surface, Neural network, Heavy metal, Chitosan beads.

Introduction

Because of their toxicity, heavy metal ions like Pb^{2+} and Ni^{2+} are known to be familiar and dangerous pollutants in the aquatic system. One of the biggest problems in the environment today is the widespread release of these pollutants from textile effluents and wastewater from other industrial processes, including pulp and paper production, leather tanning, and battery manufacturing (Banza & Rutto, 2022; Xaba et al., 2020).

In order to analyze adsorption in an aqueous mixture, numerous methods can be applied to remove this contamination from water (Igberase et al., 2017; Jakšić et al., 2021). However, for the proper design and operation of a water cleaning system, it is helpful to identify additional toxins in wastewater. Furthermore, in a multi-component system with several contaminants, they may or may not have a vital influence on the strength of the adsorbent's binding. In light of these facts, the adsorbent's binding ability

DOI: 10.6092/issn.2281-4485/18471

depends on the quantity and concentration of pollutants present in the mixture (Mokhtar et al., 2020). Subsequently, significant accomplishment has been made utilizing chitosan as a superior adsorbent to remove pollutants from water and wastewater (Igberase et al., 2017). Chitosan has unique properties that make it useful in various industries, including wastewater treatment, pharmaceuticals, medical applications, environmental protection, textiles, biotechnology, cosmetics, food processing, and agriculture. These properties include antimicrobial activity, biocompatibility, non-toxicity, and biodegradability (Mazouz et al., 2023; Mokhtar et al., 2020; Sheth et al., 2021) 2010). Chitosan is commonly made as flakes, but the formulation is not efficient in adsorption studies and results in low adsorption capacity, hence chitosan flakes are converted into beads to address the issue of poor adsorption performance. Chitosan possesses two reactive groups, which are the amino and hydroxyl groups group (Fan et al., 2013; Li et al., 2018; Liu et al., 2019; Pompeu et al., 2022), which facilitate easy graft copolymerization. In recent years, chitosan adsorbents have been broadly applied in the removal of dye and adsorbates from water in the presence of hydrogen bonding and electrostatic interactions as the most common mechanisms. Given that it is one of the most widely available, affordable polysaccharides that produces a greater number of functional groups, chitosan has been vastly exploited for the production of new hydrogels for environmental utilization (Babakhani and Sartaj, 2020; Jafarnejad et al., 2020).

The use of modeling and computer-aided simulation approaches with experimental research is applied by contemporary scientific researchers. Computer simulations can offer an understanding of the functioning correlation between the input and output parameters of the examined system or mechanistic details, depending on the modelling-tools used. The ANN used for machine learning is a crucial tool for data-driven modeling and process development of the system under investigation. However, owing to their extensive capability to model non-linear variation, RSM and ANN are used to extrapolate from historical data in order to anticipate how diverse processes would perform (Elmolla et al., 2010; Jakšić et al., 2021; Kabuba and Maliehe, 2021). Consequently, there haven't been any reports in the literature about utilizing an ANN model to simulate synthetic wastewater using chitosan derivatives. In order to determine the ideal adsorption process parameters. This study assesses the effects of process factors including pH, reaction time, starting concentration, adsorbent dose, and temperature. Based on five adsorption characteristics, the ANN model was created to forecast the adsorption of Pb^{2+} and Ni^{2+} ions. This made it possible to achieve ideal adsorption conditions. Furthermore, analysis of variance (ANOVA) was used to evaluate the statistical findings (Igberase et al., 2017; Xaba et al., 2020). The key objective of this investigation is to design a neural network model that uses experimental design matrix data from RSM-CCD to forecast the presence of adsorbates in synthetic wastewater. Additionally, SEM and FTIR were used to describe respectively the morphology and basic functional group of the developed adsorbent.

Theory of data description

To better understand how a reaction process operates and forecast relevant outcomes, simulation and modelling are process techniques that quantitatively analyse the physical surroundings of a reaction process. The foundation of deep learning is ANN, which allow a variety of computer algorithms to learn, understand, and produce educated feedback established on the root of the findings (Makomere et al., 2022; Witek-Krowiak et al., 2014). The purpose of this study is to evaluate how well ANN perform when analysing input data. However, pH, temperature, contact time, adsorbent dose, and initial concentration are input experimental factors that are taken into account in this study. Equation 1-6 was taken into consideration to highlight the importance of RSM and ANN models. Utilizing this non-linear method, predicted and actual data were compared.

$$MPSD = 100\sqrt{\frac{1}{N-P}\sum_{i=1}^{n}\left(\frac{\left(q_{e(exp)}-q_{e(pred)}\right)^{2}}{q_{e(exp)}}\right)i} \quad [1]$$

$$RMSE = \sqrt{\frac{1}{N}\sum_{i=1}^{n}\left(\frac{\left(q_{e(exp)}-q_{e(pred)}\right)^{2}}{q_{e(exp)}}\right)i} \quad [2]$$

$$\mathrm{ARE} = \frac{100}{N}\sum_{i=1}^{n}\left(\frac{\left(q_{e(exp)}-q_{e(pred)}\right)^{1}}{q_{e(exp)}}\right) \quad [3]$$

$$MSE = \frac{1}{N}\sum_{i=1}^{N}(\left|\left(q_{e(exp)} - q_{e(pred)}\right)\right|)^{2} \quad [4]$$

EQA 61 (2024): 1-15

DOI: 10.6092/issn.2281-4485/18471

$$\chi^2 = \frac{(q_{e(exp)} - q_{e(pred)})^2}{q_{e(pred)}} \quad [5]$$

$$SSE = \sum_{i=1}^{N} (|(q_{e(exp)} - q_{e(pred)})|)^2 \quad [6]$$

where N is the number of evaluations, P denotes the range of model factors, and q_e(exp) and q_e(pred) are the empirical and predicted uptake rates, accordingly.

RSM

RSM is an optimization method that examines experimental data using mathematical and statistical models. The optimization of the binding variables entails 6 crucial actions, including: (1) choosing the independent variables and responses; (2) choosing the experimental design strategy; (3) obtaining the results of the actual experiment; (4) fitting the model equation to the experimental data; (5) obtaining ANOVA; and (6) obtaining the optimal conditions (Ayoola et al., 2020; Bohlouli et al., 2016). In this study, Design-Expert Version 6.0.6 was used, and CCD was utilised to design the experiment. The design arrangement found 45 experimental runs, of which 37 of them had non-centre points and 8 had centre points using an alpha of 2. These replicas are essential because they offer independent experimental error estimation (Mokhtar et al., 2023). The quality of fit was supplied by the correlation coefficient (R^2). If the R^2 value is near to one, the model is thought to be extremely dependable. Equation [7] displays a mathematical model that the software created to represent the answer in relation to quadratic polynomial equation.

$$\gamma = \beta_o + \sum_{i=1}^{K} \beta_i X_i + \sum_{i=1}^{K} \beta_{ii} X_i^2 + \sum_{i<j} \beta_{ij} X_i X_j + e(X_1 . X_2 \ldots . X_K \quad [7]$$

where i is the linear effect, ii is the quadratic effect, and ij is the interaction effect (Xaba et al., 2020) and o is the interest variable. The positive sign in the equation indicates the variables synergistic effects. The following factors were taken into consideration as independent variables in the present investigation: pH, initial concentration, contact time, dosage, and temperature. Were Pb^{2+} and Ni^{2+} ions adsorption represented by (γ_{Pb}) and (γ_{Ni}) respectively are the response variables. CCD is used to evaluate the quadratic influences on the elimination of Pb^{2+} and Ni^{2+} ions from aqueous solutions. The model dependability is determined by the R^2 value. Using a probability less than F value, the quadratic model ability to match the experimental data can be evaluated. A probability greater than F with a value smaller than 0.0001 denotes the importance of the model term. Through ANOVA analysis and 3D model graphs, the program examined each response. Also, to examine the effects of components at multiple points in the RSM produced design and to highlight how working factors affect process efficiency, perturbation plots is utilized after validating the applicability of the empirical model.

ANN

The system based on ANN and its learning and response mechanism served as the ANN technique primary sources of inspiration. Due to its ease in estimating the degree of non-linearity, the use of ANN has been regarded as a helpful simulating device for the analysis of adsorption methods (Bohlouli et al., 2016; Cojocaru et al., 2021; Makomere et al., 2022). When modelling ANN a database is essential, the experiment is created by compiling several data points from adsorption trials. As a successful method for determining input variables, principal component analysis was used to make sure the input parameters are significant. The pre-processed experimental values are separated at random into training, testing, and validation sets based on the input and output vectors. Equation 4 represents the mean square error (MSE) and is utilised to evaluate how effective the ANN performed throughout training. Owing to the intricacy of the technique a quadratic mathematical model is chosen to describe non-linear performance. ANN approach was carried out in this study using Artificial Neural Network Toolbox V4.0, MATLAB, 2020a. In this regard, ANN might be the best method for fixing statistical problems in adsorption studies. ANN is a data processing system based on the design of a biological neural network, the input layer, hidden layer, and output layer are them three

DOI: 10.6092/issn.2281-4485/18471

levels that make up ANN. Artificial intelligence (AI) systems are built on a structure that mimics the operation of a brain network. The situations displaying linear correlations within the parameters are translated using a neural network without any hidden layers. A single-layer perceptron, which is the most basic type of neural architecture, is used to describe it. A multi-layer perceptron is a network with a hidden layer that creates a connection between the input layer and the output layer via a complex computing procedure including weight changes and activation functions. The quantity of hidden layers, which may be in shallow or deep neural networks, is determined by the complexity of the metadata. Shallow neural networks use data that does not show a straight path of correlation, such as variables that comprise several target feedbacks and have only one hidden layer (Demarchi et al., 2015; Serhan et al., 2019). ANN is regarded as a nonlinear regression technique for establishing a link between dependent and independent variables. The ANN model configuration processes involve the following steps, (1) Collecting data. (2) Train and test set selection. (3) Conversion of data into ANN inputs. (4) Identifying, training, and testing network structures. (5) If necessary, repeat the processes several times to get the best model. Due of its adaptability to noise, outliers, and overlapping data sets, ANN is thought of as being able to adapt to data with a nonlinear structure(Oladipo & Gazi, 2015). Neurons make up the layers (input layer, hidden layer, and output layer). The input layer collects independent variables, and the output layer receives dependent variables. There is no processing in the input layer, therefore it is regarded as inactive. The synaptic weights of the hidden layer, which include information pertinent to the ANN, transfer information to the output layer along the way. In order to start data transmission from the input or hidden node and to shape the computed response or output, an activation function is used, and only the online node is subject to this process. Due to its adaptability to nonlinear datasets, the hidden layer's sigmoid activation function is predominantly used by the system to compute the targeted outcome.

The time required to effectively train a network is a performance parameter that is related to the effective weight initiation. The incorrect starting weight selection may lengthen training time or potentially result in the training algorithm failing to converge. The Garson equation as shown in Equation [8] is used to determine the initial weight for ANN training (Kabuba & Banza, 2020),

$$I_j=\frac{\sum_{m=1}^{m=Nh}\left\langle\left\backslash W_{jm}^{ih}xW_{mn}^{ho}\right\backslash\right|/\sum_{k=1}^{Ni}xW_{km}^{ih}\left|W_{mn}^{ho}x\right\rangle}{\sum_{k=1}^{m=Ni}\left\langle\left\backslash W_{m=1}^{nh}xW_{mn}^{ho}\right\backslash\right|/\sum_{k=1}^{Ni}xW_{km}^{ih}\left|W_{mn}^{ho}\right\rangle} \quad [8]$$

The connection weight is W. The subscripts 'k','m', and 'n' denote input, hidden, and output neurons, respectively, and the superscripts 'I', 'h', and 'o' denote input, hidden, and output layers, respectively.

Experimental

Materials and equipment's

Without additional purification, all materials were of analytical quality. A 90% deacetylated form of chitosan powder was imported from China. Sigma-Aldrich provided aniline (99.5%). In order to graft chitosan beads, a domestic microwave was utilized. Sigma-Aldrich was used to obtain sodium hydroxide (99%), acetic acid (99%), and hydrochloric acid (99%). To alter the pH of the solution, a pH meter (Hanna HI 8421) was utilized, and it was bought from Sigma-Aldrich. In the school laboratory, distilled water was obtained using an Ultima 888 water distiller. Using an agitator (Labcon incubator), the adsorption experiment was conducted. The quantity of adsorbate ions adsorbed was calculated using a Varian spectrophotometer (Varian SpectrAA-10).

Adsorbate preparation

A calculated mass of $PbSO_4$ and $NiSO_4.6H_2O$ were separately dissolved in purified water to create the stock mixture utilized in this work. This stock mixture was then diluted to provide the necessary required concentration.

Transformation of chitosan from its powdered state

Three stages were involved in the preparation of grafted chitosan composite (MCS). The first step was to dissolve 30 g of chitosan powder in 1 L of a 10.0% (v/v) acetic acid solution. In the Second step, chitosan beads (CS) were created by passing chitosan solution using a peristaltic pump, through a glassware tube, and into a 1M sodium hydroxide so-lu-tion. To get rid of any sodium hydroxide residue,

EQA 61 (2024): 1-15

DOI: 10.6092/issn.2281-4485/18471

the beads were repeatedly washed with purified water. Thirdly, microwave irradiation was used to graft the developed beads. In an open neck flask, 5 g of chitosan beads were combined with 0.5 g/L of aniline to achieve this. Then, for 20 minutes, this flask was heated on medium-low power in a home microwave. The beads were once again washed with purified water before being applied for research use.

Characterization of the beads

Separately weighed samples of 1.0 g each of CS and MCS beads were oven dried at 60 °C before being blended to create a powder. A Shimadzu FTIR model 8300 was used for the infrared measurement, and spectra between 500 and 4000 cm^{-1} were collected. To clearly see the interior fibers, the SEM examination was carried out by bisecting CS and MCS beads separately and coating them with gold. The gold-coated beads were analyzed using a Jeol 733 super probe.

Adsorption studies

Batch studies were conducted to develop the adsorption technique and was carried out in a 200 mL glass stoppered Erlenmeyer flasks holding test solutions at the necessary level of Ni^{2+} and Pb^{2+} ions concentration of 50-150 mg/L, reaction time of 10-100 min, pH of 1-8, adsorbent dosage of 1-8g and temperatures of 25-55 °C. In each test, 100 mL of a solution containing Ni^{2+} and Pb^{2+} ions at a particular concentration were added to each flask. Using diluted 0.1 M HCl/NaOH, the pH of the solution was adjusted to maintain the required pH throughout the experiment. The required amount of adsorbent was added, and the solution was shaken at 120 rpm. Centrifugation was then used to separate the solid and liquid phases for 10 min at 2500 rpm. The removal percentage (%) was assessed using Equation [9].

$$percentage\ removal = \frac{C_o - C_e}{C_o} x100 \quad [9]$$

where C_o and C_e (mg/L) denotes the initial and final concentration respectively.

Outcomes and discussion

Characterization of the beads

FTIR analysis. To examine the structure, basic functional group and chemical bond of materials, FTIR spectra was utilized. Figure 1 elucidates the FTIR spectra of CS and MCS beads respectively. In this illustration, it can be seen that CS has functional groups that are typical of glycosidic material on its surface. The features of CS are visible in the spectrum. The existence of exchangeable protons from the hydroxyl and amine group is shown by a band at 3390 cm^{-1}. A peak at wavelength 2841 cm^{-1} in the aliphatic range (2800-3000 cm^{-1}) is attributed to asymmetric -CH_2 stretching (Chen et al., 2022; Jiang et al., 2019). The IR spectrum displayed a peak at 1000 cm^{-1}, which is a representation of oxygenated functional groups from aliphatic ethers and alcohols (Tirtom et al., 2012). Ketone and amide C=O stretching vibrations are thought to be responsible for the peak at 1541 cm^{-1}. CS properties were clearly altered when it was grafted with aniline, indicating that this process altered its characteristics. The main difference in the peaks are, (i) a shift to the left in the broad band from 3390 to 3348 cm^{-1}. (ii) a peak that was moved to the left from 1541 to 1579 cm^{-1}; (iii) left shift from 1415 to 1515 cm^{-1}; and (iv) a shift to the left, from 1000 to 1010 cm^{-1}. This observation in the shifting of the peaks may be due to the strong bond that originated owning to chemical linkage between aniline and CS. Another evidence of successful grafting is seen in the enhanced intensity between 1200 cm^{-1} to 1500 cm^{-1}. The existence of OH, and NH_2 groups contributes to the high binding capability of this ligand. These groups are prone to the development of metal complexes.

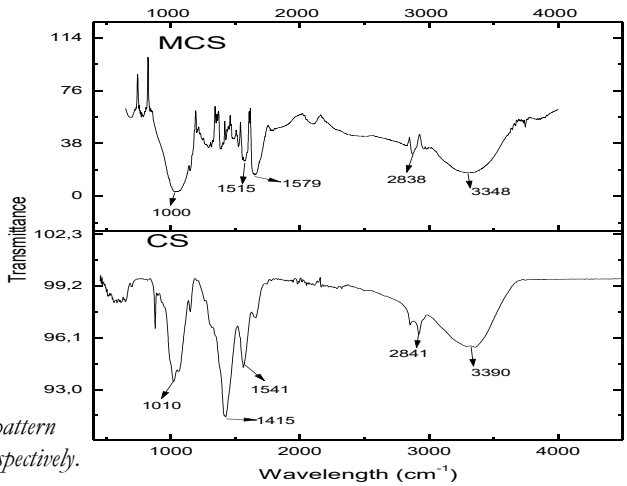

Figure 1. *FTIR pattern of CS and MCS respectively.*

EQA 61 (2024): 1-15

DOI: 10.6092/issn.2281-4485/18471

SEM results. The morphology and modifications of chitosan following grafting were examined using SEM. Figure 2 displays SEM pictures of the distinct set of beads. Subsequently, on grafting aniline onto the backbone of CS, the surface of MCS appeared to be smoother and more visible than that of CS as a result of the interaction between native chitosan solution and aniline.

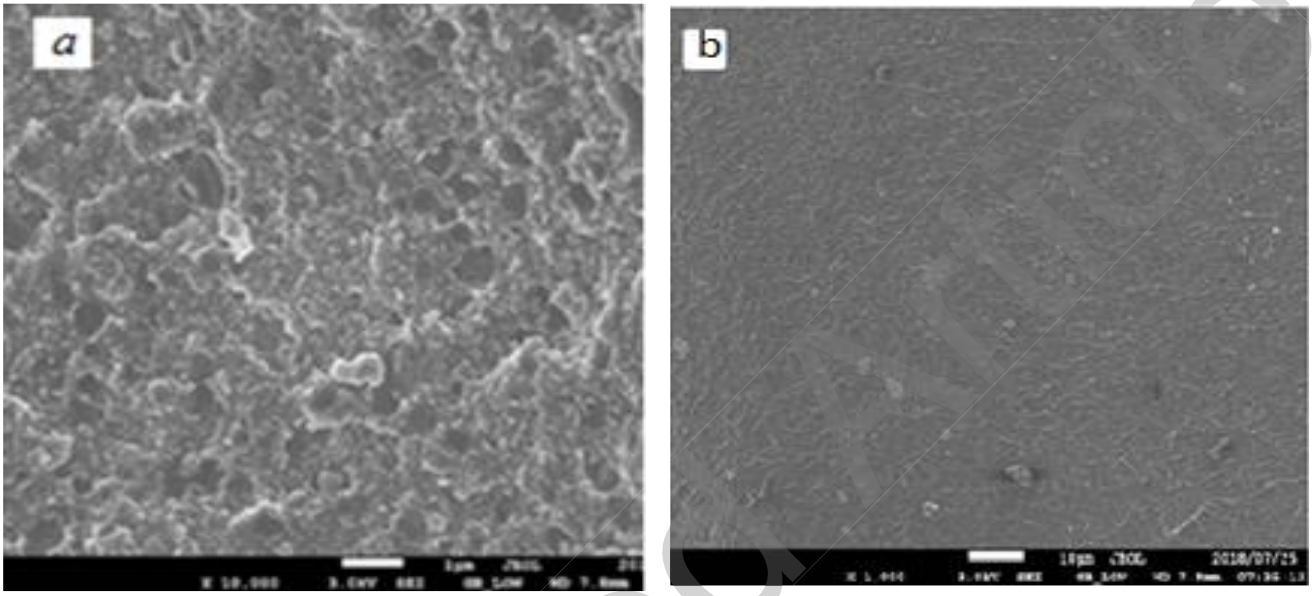

Figure 2. *SEM images of (a) CS, (b) MCS respectively*

RSM results

Table 1 shows the experimental design matrix as well as their responses to the binding of metal ions onto adsorbent. This table makes clear the impact of various parameters on the outcomes. As operational conditions vary, significant variances are also seen to occur. The small discrepancy between the predicted and actual values and the similarity provided evidence that the model was adequate. The final quadratic polynomial equation in Equations [10] and[11], where pH, reaction time, adsorbate concen-tration, temperature, and adsorbent dose are each denoted by A, B, C, D, and E, provides the coded factors that were utilized to match the experiment data. The design matrix was well-fitted, and the model was extremely dependable, according to the firm correlation coefficients (R^2) in the experimental and predicted values which were 0.987 and 0.984 for Pb^{2+} and Ni^{2+} ions respectively.

$$\gamma_{Pb} = +94.19 + 2.19A + 1.08B + 2.52C + 3.95D + 6.04E - 14.96A^2 - 1.84B^2 2.45C^2 - 0.99D^2 - 3.47E^2 - 0.15AB - 0.52AC + 0.73AD + 0.36AE - 0.49BC - 0.66BD - 0.92BE - 195CD - 1.83CE - 1.11DE \quad \textbf{[10]}$$

$$\gamma_{Ni} = +94.19 + 2.20A + 1.10B + 2.54C + 3.96D + 6.05E - 14.95A^2 - 1.85B^2 - 2.46C^2 - 0.99D^2 - 3.48E^2 - 0.17AB - 0.54AC + 0.72AD + 0.34AE - 0.50BC - 0.68BD - 0.93BE - 1.97CD - 1.85CE - 1.12DE \quad \textbf{[11]}$$

DOI: 10.6092/issn.2281-4485/18471

Table 1. *Design matrix and response*

STD	Facror 1 A: pH	Factor 2 B: Reaction time (min)	Factor 3 C: Adsorbate concentration (mg/L)	Factor 4 D:Temperatue (°C)	Factor 5 E: Adsorbent dose (g)	Response 1; Pb^{2+} removal (%)	Response 2: Pb^{2+} removal (%)
1	2.00	10.00	50.00	25.00	1.00	48.14	47.67
2	8.00	10.00	50.00	25.00	1.00	51.70	51.00
3	2.00	100.00	50.00	25.00	1.00	54.78	54.75
4	8.00	100.00	50.00	25.00	1.00	57.79	57.69
5	2.00	10.00	150.00	25.00	1.00	62.91	62.79
6	8.00	10.00	150.00	25.00	1.00	64.44	64.24
7	2.00	100.00	150.00	25.00	1.00	67.97	67.44
8	8.00	100.00	150.00	25.00	1.00	68.57	68.28
9	2.00	10.00	50.00	55.00	1.00	62.64	62.02
10	8.00	10.00	50.00	55.00	1.00	68.99	68.50
11	2.00	100.00	50.00	55.00	1.00	66.01	65.98
12	8.00	100.00	50.00	55.00	1.00	71.98	71.85
13	2.00	10.00	150.00	55.00	1.00	68.97	68.85
14	8.00	10.00	150.00	55.00	1.00	73.65	73.22
15	2.00	100.00	150.00	55.00	1.00	71.43	70.86
16	8.00	100.00	150.00	55.00	1.00	74.98	74.63
17	2.00	10.00	50.00	25.00	6.00	67.88	57.22
18	8.00	10.00	50.00	25.00	6.00	72.99	72.21
19	2.00	100.00	50.00	25.00	6.00	71.67	70.14
20	8.00	100.00	50.00	25.00	6.00	74.85	74.52
21	2.00	10.00	150.00	25.00	6.00	74.99	74.54
22	8.00	10.00	150.00	25.00	6.00	77.95	77.42
23	2.00	100.00	150.00	25.00	6.00	75.98	75.52
24	8.00	100.00	150.00	25.00	6.00	78.65	77.79
25	2.00	10.00	50.00	55.00	6.00	75.97	76.67
26	8.00	10.00	50.00	55.00	6.00	78.88	84.58
27	2.00	100.00	50.00	55.00	6.00	77.56	76.95
28	8.00	100.00	50.00	55.00	6.00	76.99	84.25
29	2.00	10.00	150.00	55.00	6.00	85.44	76.17
30	8.00	10.00	150.00	55.00	6.00	77.89	81.98
31	2.00	100.00	150.00	55.00	6.00	82.56	74.51
32	8.00	100.00	150.00	55.00	6.00	75.42	79.70
33	5.00	100.00	100.00	40.00	6.00	81.66	88.99
34	5.00	55.00	150.00	40.00	3.50	88.98	88.89
35	5.00	55.00	100.00	10.00	3.50	89.88	89.42
36	5.00	55.00	100.00	40.00	3.50	82.58	82.33
37	5.00	55.00	100.00	40.00	8.50	98.14	98.12
38	5.00	55.00	100.00	40.00	3.50	92.97	92.39
39	5.00	55.00	100.00	40.00	3.50	94.79	94.19
40	5.00	55.00	100.00	40.00	3.50	94.79	94.19
41	5.00	55.00	100.00	40.00	3.50	94.70	94.19
42	5.00	55.00	100.00	40.00	3.50	94.68	94.19
43	5.00	55.00	100.00	40.00	3.50	94.68	94.19
44	5.00	55.00	100.00	40.00	3.50	94.68	94.19
45	5.00	55.00	100.00	40.00	3.50	94.68	94.19

Using analysis of variance (ANOVA), it determined how pH, adsorbate concentration, temperature, adsorbent dose, and reaction time affected the removal efficiency of Pb^{2+} and Ni^{2+} ions. Consequently, at a 95% confidence level, a P-value of less than 0.05 shows statistical relevance. In this instance, important model terms include A, B, C, D, E, A^2, B^2, C^2, D^2, E^2, AB, AC, AD, AE, BC, BD, BE, CD, CE, and DE. Pb^{2+} and Ni^{2+} ions are indicated by the ANOVA statistical results in Tables 2 and 3, respectively and appeared to be similar. The relevance of the model in characterizing the experi-

DOI: 10.6092/issn.2281-4485/18471

Table 2. *% Pb^{2+} Removal ANOVA for Response Surface Quadratic Model*

Source	Sum of Squuares	DF	Mean Square	F-Values	Prof > F
Model Signicant	7143.17	20	357.16	6.693E+006	< 0.0001
A	152.99	1	152.99	2.867E+006	< 0.0001
B	37.48	1	37.48	7.023E+005	< 0.0001
C	203.67	1	203.67	3.817E+006	< 0.0001
D	623.55	1	623.55	1.169E+007	< 0.0001
E	1166.08	1	1166.08	2.185E+007	< 0.0001
A^2	818.90	1	818.90	1.153E+007	< 0.0001
B^2	43.39	1	43.39	8.131E+005	< 0.0001
C^2	77.08	1	77.08	1.444E+006	< 0.0001
D^2	25.03	1	25.03	4.690E+005	< 0.0001
E^2	153.97	1	153.97	2.886E+005	< 0.0001
AB	0.75	1	0.75	14004.16	< 0.0001
AC	8.81	1	8.81	1.651E+005	< 0.0001
AD	17.10	1	17.10	3.204E+006	< 0.0001
AE	4.13	1	4.13	77317.77	< 0.0001
BC	7.58	1	7.58	1.402E+005	< 0.0001
BD	14.03	1	14.03	2.630E+005	< 0.0001
BE	27.10	1	27.10	5.079E+005	< 0.0001
CD	122.19	1	122.19	2.290E+006	< 0.0001
CE	10313	1	10313	2.008E+006	< 0.0001
DE	39.18	1	39.18	7.343E+005	< 0.0001
Residual	1.281E-003	24	5.336E-005		
Lack of fit	1.281E-003	17	7.533E-005		
Pure error	0.000	1	0.000		
Core total	7143.17	44			

Table 3. *% Ni^{2+} Removal ANOVA for Response Surface Quadratic Model*

Source	Sum of Squuares	DF	Mean Square	F-Values	Prof > F
Model Signicant	7143.17	20	357.16	6.693E+006	< 0.0001
A	152.99	1	152.99	2.867E+006	< 0.0001
B	37.48	1	37.48	7.023E+005	< 0.0001
C	203.67	1	203.67	3.817E+006	< 0.0001
D	623.55	1	623.55	1.169E+007	< 0.0001
E	1166.08	1	1166.08	2.185E+007	< 0.0001
A^2	818.90	1	818.90	1.153E+007	< 0.0001
B^2	43.39	1	43.39	8.131E+005	< 0.0001
C^2	77.08	1	77.08	1.444E+006	< 0.0001
D^2	25.03	1	25.03	4.690E+005	< 0.0001
E^2	153.97	1	153.97	2.886E+005	< 0.0001
AB	0.75	1	0.75	14004.16	< 0.0001
AC	8.81	1	8.81	1.651E+005	< 0.0001
AD	17.10	1	17.10	3.204E+006	< 0.0001
AE	4.13	1	4.13	77317.77	< 0.0001
BC	7.58	1	7.58	1.402E+005	< 0.0001
BD	14.03	1	14.03	2.630E+005	< 0.0001
BE	27.10	1	27.10	5.079E+005	< 0.0001
CD	122.19	1	122.19	2.290E+006	< 0.0001
CE	10313	1	10313	2.008E+006	< 0.0001
DE	39.18	1	39.18	7.343E+005	< 0.0001
Residual	1.281E-003	24	5.336E-005		
Lack of fit	1.281E-003	17	7.533E-005		
Pure error	0.000	1	0.000		
Core total	7143.17	44			

EQA 61 (2024): 1-15

DOI: 10.6092/issn.2281-4485/18471

mental data is confirmed by the high F-values (6693453.81 for Pb^{2+} ions and 6693453.12 for Ni^{2+} ions), respectively. A "Model F-value" this large may happen by accident only 0.01% of the time. The modified R^2 value for Pb^{2+} and Ni^{2+} ions and the expected value are in agreement. The precision analysis resulted in a ratio of 813.789, which suggested a sufficient signal for this work. The relationship between the removal efficiency of the predicted and actual values of Pb^{2+} and Ni^{2+} ions is shown in Figures 3a and b. It can be seen from the graph that the majority of the data points were clustered closely together around the straight line of best fit. This progression demonstrates consistency between the predicted and experimental data, supporting the model's importance (Banza & Rutto, 2022; Witek-Krowiak et al., 2014) The effect of each variable on removal efficiency was clarified using the perturbation plot (Figure 4a and b).

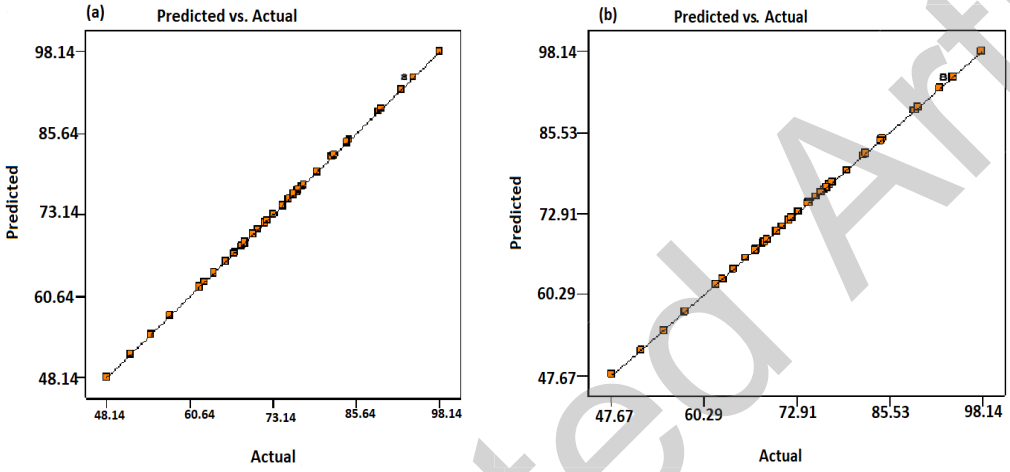

Figure 3
Predicted removal efficiency from model against the experimental efficiency.

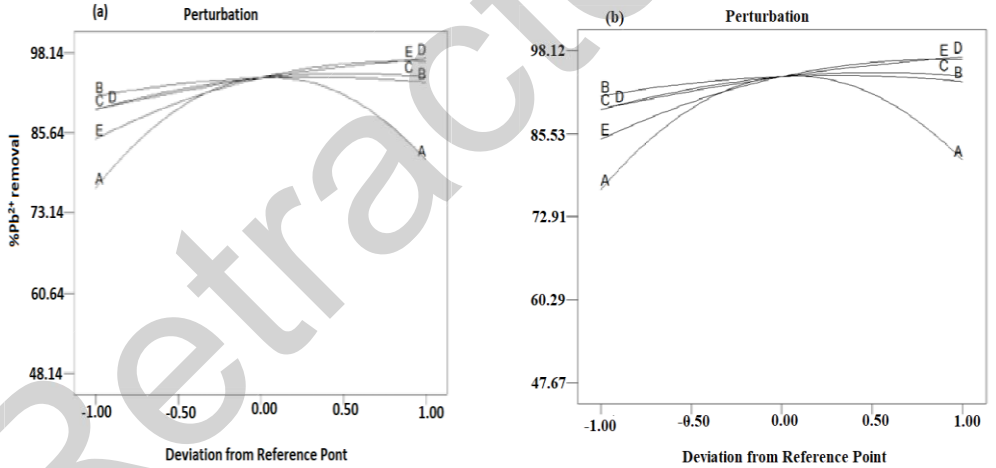

Figure 4
Perturbation graphs showing the impact of each variable on removal efficiency.

Perturbation is the independent variable's resultant variation in removal efficiency from the reference point. The reference point was based on the following parameters: pH 5, 55 min, 40 °C, 6.0 g of adsorbent, and 150 mg/L of adsorbate. It was shown from this plot that each variable increased removal efficiency in a proportionate manner until it reached its maximum value, at which point an additional increase had no appreciable impact. Additionally, the plot shows that each variable concave shape with regard to removal efficiency is caused by a large quadratic factor (Igberase et al., 2017) Figure 5 (a-f) displays the findings from the 3D response surface study. These graphs demonstrate how two variables affect removal efficiency while holding the other variables constant. This Figure shows how the parameters affect the removal efficiency. The plots show that the highest adsorbate removal occurs for reaction times of 55 min, pH 5, 6.0 g of adsorbent, 150 mg/L of adsorbate, and 40 °C. These results are

DOI: 10.6092/issn.2281-4485/18471

consistent with the literature (Ayoola et al., 2020; Bohlouli et al., 2016; Igberase et al., 2017) The fact that the highest adsorption in these figures occurred at pH 5 demonstrates the critical role that pH plays in the adsorption of Pb^{2+} and Ni^{2+} ions onto MCS. According to (Zhang et al., 2022), pH is a key factor in cation adsorption because it affects both the ionization of chemically active sites on the adsorbent surface and the chemical speciation of metals in solution. However, at low pH, hydrogen ions are abundant on the surface of the MCS, which prevents metal ions from adhering due to competition for binding sites and a reduction in removal efficiency. Maximum pH was reached at 5 for both metals because as pH rises, competition decreases in favour of adsorption. Increasing the pH above 6 leads to precipitation of the insoluble Pb^{2+} and Ni^{2+} ions hydroxide which results in low removal efficiency According to Figure 5(b, e), another factor that significantly affects the binding of both metal ions is the dosage of the adsorbent. In these two figures, it can be seen that the removal efficiency increases as the dosage is increased. This behaviour might be brought on by the presence of enough sites for metal ion binding. A higher adsorbent dosage can also force a reduction in the charge of the dense outer layer of the cells, which can block the adsorption sites for both metal ions removal, which can be attributed to the overlapping of adsorption sites as a result of saturated adsorbent particles (Jakšić et al., 2021; Kabuba & Banza, 2020). The overall conclusion that removal efficiency is a function of all the variables examined in the present work may be drawn from each plot.

Levenberg-Marquardt (LM) algorithm modelling analysis for ANN

In this study, the network parameters were changed to alter the coding process circumstances for LM. During data simulations, the LM was limited to 10 data passes at most. In the LM training, there was no early stopping mechanism employed. Figure 6 displays the ANN regression plot for training, validation, test, and overall, together with the high corelation coefficient of the Pb^{2+} and Ni^{2+} ions (R close to 1 and equal to 1). This algorithm's computation methods ensure that it can adapt to noisy data sets. After 50 iterations and 16 completed epochs, the LM model had received enough training. Validation tests were run using the LM algorithm (Witek-Krowiak et al., 2014), the LM algorithm performs well and learns quickly (Biglarijoo et al., 2017; Elmolla et al., 2010; Oladipo & Gazi, 2015). LM's validation tests are crucial for identifying weight inaccuracies that might have occurred during training. The LM algorithm's starting weights as obtained from Equation 8, are as follows: [1.1231; 1.3242; 1.3543; 1.3876; 0.6765; 1.1276; 1.643; 0.3543; 1.4324; 1.1242]. The decision to use the LM algorithm was influenced by these weights. The MSE produced by combining this algorithm with weights has the lowest MSE of 0.000062, indicating that this algorithm has very little error. The training session was shortened by these weights. The values for training, validation, and test 'R' were all equal to 0.9992, and it produced a distinct straight line. Similar to the RSM method, the experimental runs were split into 70, 15 and 15% portions for training, validation, and testing, and these portions were then transferred to the ANN model. As depicted in figure 6, while figure 7 depicts how the network interacts with the training, testing, and validation data. Correlation coefficients for training, testing, validation, and total data were found to be 1, 0.96837, 0.96146, and 0.98994, respectively. The straight line also demonstrates a linear relationship. The experimental (target) data and the predicted (output) data from the model correlate. The results suggest that there is good agreement between the real data and the data predicted by the model. The coefficient of overall correlation therefore reveals the excellent prediction capacity of the developed ANN model and is suitable for properly forecasting data. The plots of error analysis, which include the mean square error and error histogram, are shown in Figure 8. The adsorption procedure had the least error, measuring -0.2832, according to the error histogram with 20 bins. The ANN model used a structure of 5-10-2 because of its 5 input parameters, 10 hidden layers, and 2 replies (output). Its number of neurons was discovered to be 10 after 50 iterations. As seen in figure 9, the effectiveness of the ANN during training is evaluated using MSE. According to the research of the MSE's mono-layered architecture, performance improved with increasing order. After many trial and error runs, the trained network's best removal efficiency performance was 17.3472 at epoch 10 for the MSE analysis. It was discovered that this value enables stable and quick learning.

DOI: 10.6092/issn.2281-4485/18471

Three-dimensional (3D) RSM plots

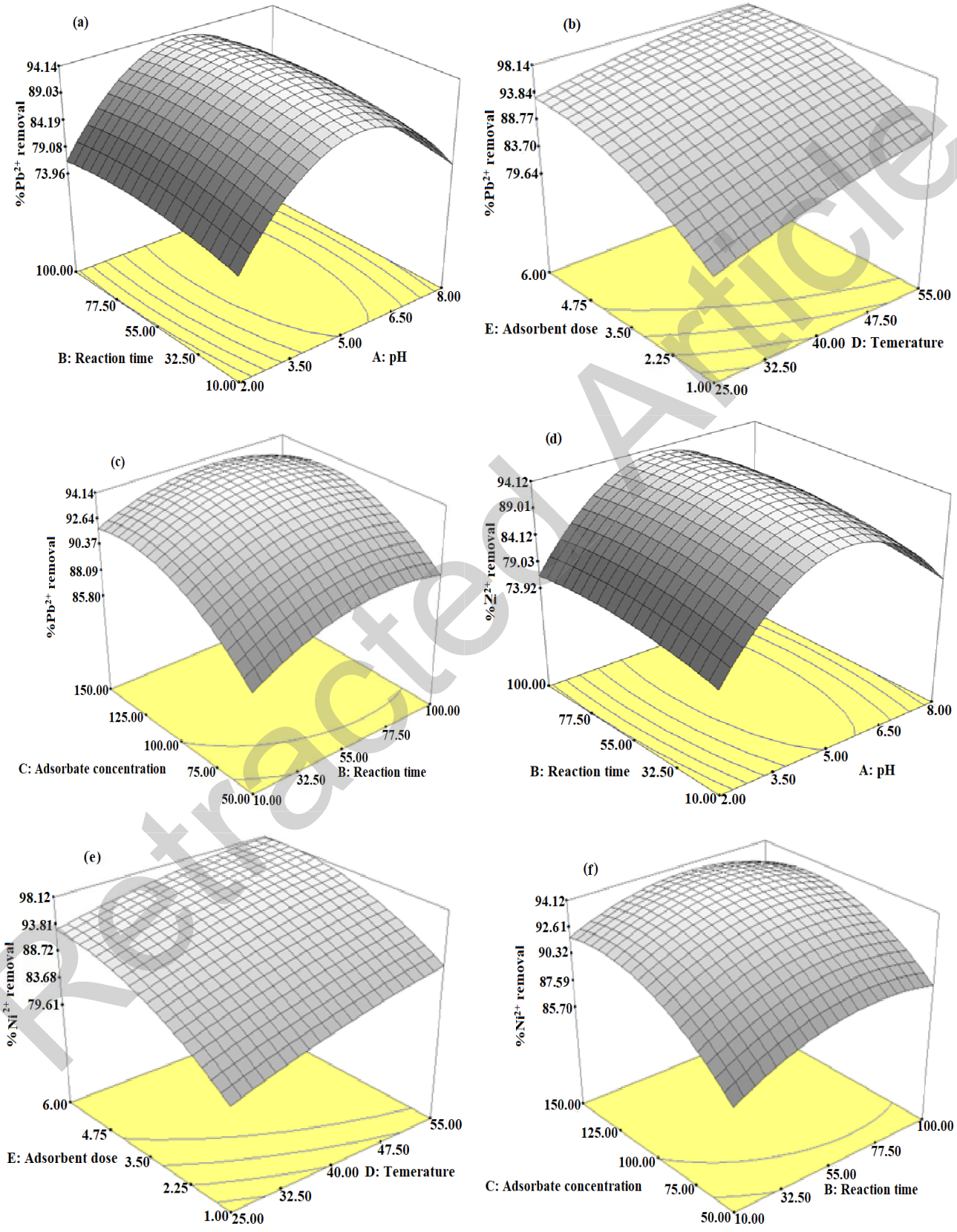

Figure 5a-f. *Three-dimensional (3D) RSM graphs*

EQA 61 (2024): 1-15

DOI: 10.6092/issn.2281-4485/18471

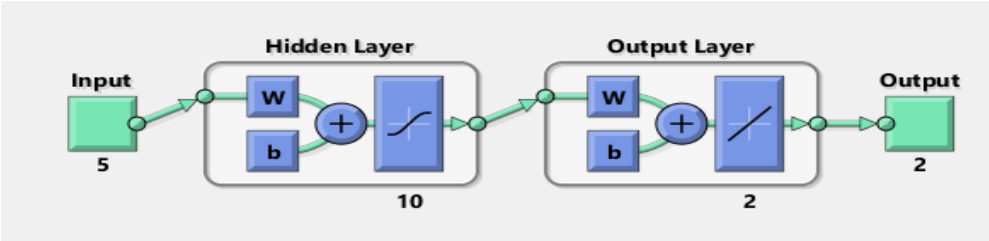

Figure 6
ANN architecture and LM algorithm in predicting removal efficiency of metal ions by MCS.

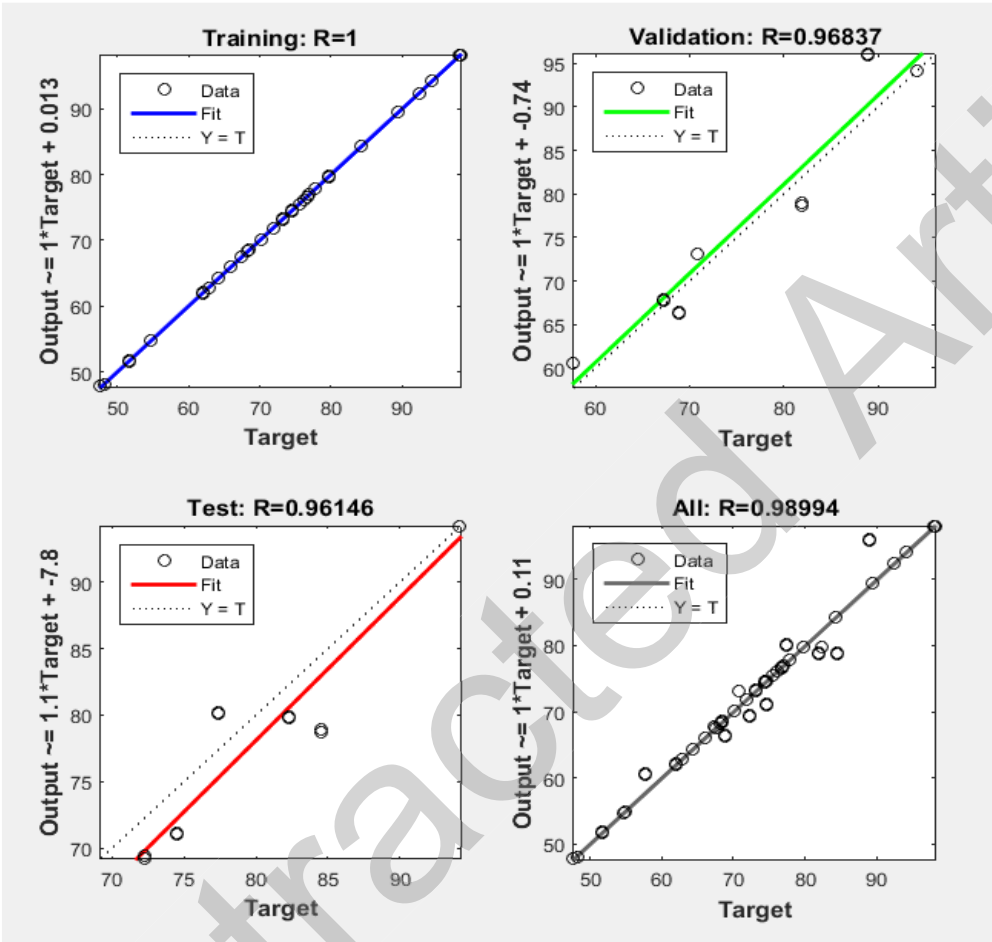

Figure 7
Regression plot describing graphical representation for Levenberg-Marquardt

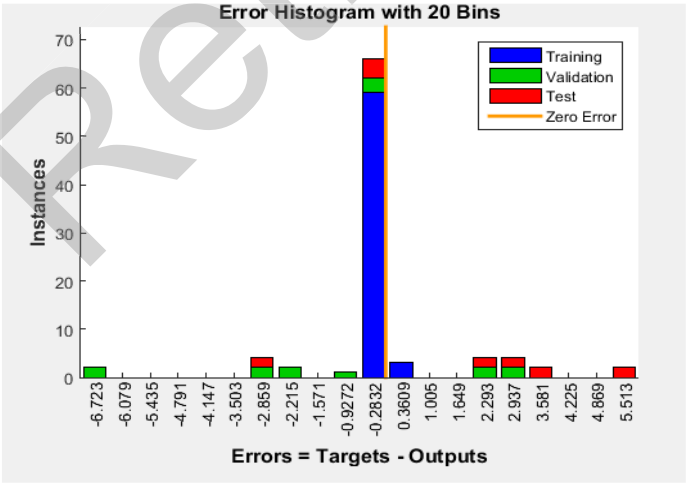

Figure 8. *ANN error histogram analysis for metal ions adsorption*

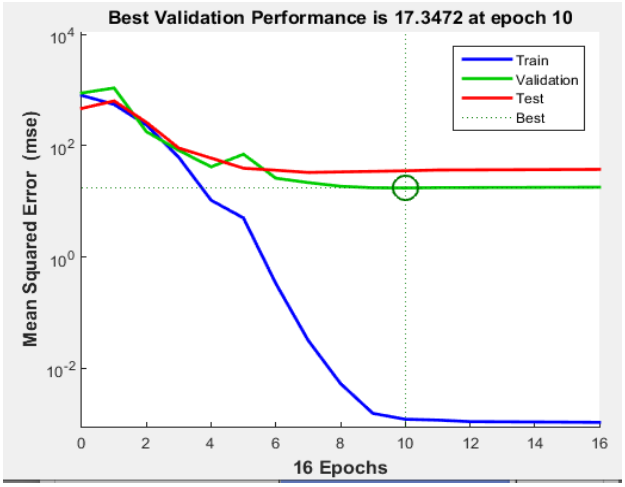

Figure 9. Performance graph for Levenberg-Marquardt at epochs 16.

EQA 61 (2024): 1-15

DOI: 10.6092/issn.2281-4485/18471

The prediction accuracy of developed ANN and RSM models

One experiment was evaluated at the level of the process parameters, as indicated in Table 4, and ANN and RSM models were evaluated for the prediction of metal ions removal effectiveness (%). The comparison of actual and expected removal efficiencies (%) showed that ANN and RSM models have a promising capacity to forecast values that are noticeably near to actual values. To compare statistically the adequacy of both models, the statistical significance and error distribution of removal (%) efficiencies predicted by RSM and ANN were further evaluated. The coefficient of determination (R^2) is seen as the most common statistical metric for evaluating the accuracy of a prediction. This method focuses on the linear correlations between the experimental data and the model's predictions. This method offers no information regarding nonlinear relationships or error distribution. Therefore, to ascertain the magnitude and measure errors distribution, the non-linear statistic metrics were used. This outcome is shown in Table 5, which calculates the differences between experimental and anticipated Pb^{2+} and Ni^{2+} levels using the RSM and ANN approaches, respectively. Despite this, the R2 values for the two models are near to one another, indicating that the predictions are more in line with the actual values. When compared to RSM, a lower error function value was obtained for ANN. Therefore, according to statistical criteria, ANN outperforms RSM in terms of model predictions. In comparison, the ANN model's statistical metrics and prediction capabilities outperformed the RSM model. Therefore, applications of ANN and RSM techniques for modelling and optimizing the adsorption process are validated based on the outstanding accuracy of the projected responses.

A	B	C	D	E	Actual Removal %	Predicted removal (ANN) %	Predicted removal (RSM) %
5	55	100	40	6	98.14	98.17	98.65

Table 4
Comparison between the experimental and predicted values of Pb^{2+} ions removal efficiency by ANN and RSM.

Error function	ANN	RSM
Marquart's percent standard deviation (MPSD)	0.0065	0.0532
Chi-square test (χ^2)	0.0022	0.0411
Root means square error (RMSE)	0.0036	0.0732
Mean squared error (MSE)	0.0002	0.0011
Sum of the squares of errors (SSE)	0.0005	0.0031
Average relative errors (ARE)	0.0062	0.0320

Table 5
Non-linear error functions list as statistical measure fit for ANN and RSM.

Conclusion

Simulation experiments utilizing RSM and ANN were carried out in the current research to assess the removal efficiency of Pb^{2+} and Ni^{2+} ions in aqueous solution. In RSM experimental data, CCD was used, and in ANN, LM training network was utilised in the backpropagation approach. Five input layer neurons and two output layer neurons make up various ANN architectures that are based on hidden layer trigger algorithms and hidden layer cells for LM coding. Using error functions and goodness of fit (R^2) analysis, a comparative evaluation of the removal efficiency prediction performance was conducted. Both models accurately predicted the removal efficiency of metal ions. To forecast the adsorption of Pb^{2+} and Ni^{2+} ions in aqueous solution, a three-layer backpropagation neural network was optimized. With a correlation coefficient (R^2) of 0.997 and an MSE of 0.00006, the experimental result and the result predicted by RSM and ANN are highly similar. The results of the sensitivity analysis demonstrated that the adsorption process is strongly influenced by all of the examined variables (reaction time, temperature, pH, adsorbent mass, and adsorbate concentration). Results from RSM-CCD and ANN demonstrated the modelling capacity to accurately simulate and predict process behaviour. ANN model performed better with regards to statistical analysis and R^2 values. Pb^{2+} and

DOI: 10.6092/issn.2281-4485/18471

Ni^{2+} ions model equations were created utilizing sets of experimental data. The experimental results and the projected values agreed very well. The relevance of the model was described using the model equations. The characterisation outcomes for both unmodified and modified chitosan beads were noteworthy. These results suggest that modified chitosan beads may be effective at removing metal ions from wastewater.

References

AYOOLA A. A., HYMORE F. K., OMONHINMIN C. A., BABALOLA P. O., FAYOMI O. S. I., OLAWOLE O. C., OLAWEPO A. V., BABALOLA A. (2020) Response surface methodology and artificial neural network analysis of crude palm kernel oil biodiesel production. Chemical Data Collections, 28. https://doi.org/10.1016/j.cdc.2020.100478

BABAKHANI A., SARTAJ M. (2020) Removal of Cadmium (II) from aqueous solution using tripolyphosphate cross-linked chitosan. Journal of Environmental Chemical Engineering, 8(4). https://doi.org/10.1016/j.jece.2020.103842

BANZA M., RUTTO H. (2022) Modelling of adsorption of nickel (II) by blend hydrogels (cellulose nanocrystals and corn starch) from aqueous solution using adaptive neuro-fuzzy inference systems (ANFIS) and artificial neural networks (ANN). Canadian Journal of Chemical Engineering. https://doi.org/10.1002/cjce.24603

BIGLARIJOO N., MIRBAGHERI S. A., BAGHERI M., EHTESHAMI M. (2017) Assessment of effective parameters in landfill leachate treatment and optimization of the process using neural network, genetic algorithm and response surface methodology. Process Safety and Environmental Protection, 106: 89–103. https://doi.org/10.1016/j.psep.2016.12.006

BOHLOULI A., AFSHAR M. R., ABOUTALEBI M. R., SEYEDEIN S. H. (2016) Optimization of tungsten leaching from low manganese wolframite concentrate using Response Surface Methodology (RSM). International Journal of Refractory Metals and Hard Materials, 61:107–114. https://doi.org/10.1016/j.ijrmhm.2016.07.012

CHEN J., DONG R., CHEN S., TANG D., LOU X., YE C., QIU T., YAN W. (2022) Selective adsorption towards heavy metal ions on the green synthesized polythiophene/MnO2 with a synergetic effect. Journal of Cleaner Production, 338. https://doi.org/10.1016/j.jclepro.2022.130536

COJOCARU C., HUMELNICU A. C., PASCARIU P., SAMOILA P. (2021) Artificial neural network and molecular modeling for assessing the adsorption performance of a hybrid alginate-based magsorbent. Journal of Molecular Liquids, 337. https://doi.org/10.1016/j.molliq.2021.116406

DEMARCHI C. A., DEBRASSI A., MAGRO J. D., NEDELKO N., ŚLAWSKA-WANIEWSKA A., DŁUZEWSKI P., GRENECHE J. M., RODRIGUES C. A. (2015) Adsorption of Cr(VI) on crosslinked chitosan-Fe(III) complex in fixed-bed systems. Journal of Water Process Engineering, 7: 141–152. https://doi.org/10.1016/j.jwpe.2015.05.003

ELMOLLA E. S., CHAUDHURI M., ELTOUKHY M. M. (2010) The use of artificial neural network (ANN) for modeling of COD removal from antibiotic aqueous solution by the Fenton process. Journal of Hazardous Materials, 179(1–3): 127–134. https://doi.org/10.1016/j.jhazmat.2010.02.068

FAN L., LUO C., SUN M., LI X., QIU, H. (2013) Highly selective adsorption of lead ions by water-dispersible magnetic chitosan/graphene oxide composites. Colloids and Surfaces B: Biointerfaces, 103:523–529. https://doi.org/10.1016/j.colsurfb.2012.11.006

IGBERASE E., OSIFO P., OFOMAJA A. (2017) Chromium (VI) ion adsorption by grafted cross-linked chitosan beads in aqueous solution–a mathematical and statistical modeling study. Environmental Technology (United Kingdom), 38(24): 3156–3166. https://doi.org/10.1080/09593330.2017.1290152

JAFARNEJAD M., ASLI M.D., TAROMI F.A., MANOOCHEHRI M. (2020) Synthesis of multi-functionalized Fe3O4-NH2-SH nanofiber based on chitosan for single and simultaneous adsorption of Pb(II) and Ni(II) from aqueous system. International Journal of Biological Macromolecules, 148: 201–217. https://doi.org/10.1016/j.ijbiomac.2020.01.017

JAKŠIĆ O. M., JAKŠIĆ Z., SILVA A. G. (2021) Comparing artificial neural network algorithms for prediction of higher heating value for different types of biomass. https://doi.org/10.21203/rs.3.rs-267108/v1

JIANG C., WANG X., WANG G., HAO C., LI X., LI, T. (2019) Adsorption performance of a polysaccharide composite hydrogel based on crosslinked glucan/chitosan for heavy metal ions. Composites Part B: Engineering, 169: 45–54. https://doi.org/10.1016/j.compositesb.2019.03.082

KABUBA J., BANZA M. (2020) Ion-exchange process for the removal of Ni (II) and Co (II) from wastewater using modified clinoptilolite: Modeling by response surface methodology and artificial neural network. Results in Engineering, ttps://doi.org/10.1016/j.rineng.2020.10018909

DOI: 10.6092/issn.2281-4485/18471

KABUBA J., MALIEHE A. V. (2021) Application of neural network techniques to predict the heavy metals in acid mine drainage from South African mines. Water Science and Technology, 84(12):3489–3507. https://doi.org/10.2166/wst.2021.494

LI L., IQBAL J., ZHU Y., ZHANG P., CHEN W., BHATNAGAR A., DU Y. (2018) Chitosan/Ag-hydroxyapatite nanocomposite beads as a potential adsorbent for the efficient removal of toxic aquatic pollutants. International Journal of Biological Macromolecules, 120:1752–1759. https://doi.org/10.1016/j.ijbiomac.2018.09.190

LIU Y., HU L., TAN B., LI J., GAO X., HE Y., DU X., ZHANG W., WANG W. (2019) Adsorption behavior of heavy metal ions from aqueous solution onto composite dextran-chitosan macromolecule resin adsorbent. International Journal of Biological Macromolecules, 141: 738–746. https://doi.org/10.1016/j.ijbiomac.2019.09.044

MAKOMERE R., RUTTO H., KOECH L., BANZA M. (2022) The use of Artificial Neural Network (ANN) in Dry Flue Gas Desulphurization Modelling: Levenberg-Marquardt (LM) and Bayesian Regularization (BR) algorithm comparison. Canadian Journal of Chemical Engineering. https://doi.org/10.1002/cjce.24715

MAZOUZ F., ABDELKRIM S., MOKHTAR A., ZAHRAOUI M., ABDELMOUMÈNE B., FOUATIH S. L., HASNAOUI M. A., BENGUEDDACH A., SASSI M., DJELAD A. (2023) Removal of Cu(II) Ions from Aqueous Solutions Using Chitosan/Zeolite Composites: Effects of the Size of the Beads and the Zeolitic Content. Journal of Polymers and the Environment, 31(1), 193–209. https://doi.org/10.1007/s10924-022-02622-y

MOKHTAR A., ABDELKRIM S., BOUKOUSSA B., HACHEMAOUI M., DJELAD A., SASSI M., ABBOUD M. (2023) Elimination of toxic azo dye using a calcium alginate beads impregnated with NiO/activated carbon: Preparation, characterization and RSM optimization. International Journal of Biological Macromolecules, 233. https://doi.org/10.1016/j.ijbiomac.2023.123582

MOKHTAR A., ABDELKRIM S., DJELAD A., SARDI A., BOUKOUSSA B., SASSI M., BENGUEDDACH A. (2020) Adsorption behavior of cationic and anionic dyes on magadiite-chitosan composite beads. Carbohydrate Polymers, 229. https://doi.org/10.1016/j.carbpol.2019.115399

OLADIPO A. A., GAZI M. (2015) Nickel removal from aqueous solutions by alginate-based composite beads: Central composite design and artificial neural network modeling. Journal of Water Process Engineering, 8:e81–e91. https://doi.org/10.1016/j.jwpe.2014.12.002

POMPEU L. D., MURARO P. C. L., CHUY G., VIZZOTTO B. S., PAVOSKI G., ESPINOSA D. C. R., DA SILVA FERNANDES L., DA SILVA W. L. (2022) Adsorption for rhodamine b dye and biological activity of nano-porous chitosan from shrimp shells. Environmental Science and Pollution Research, 29(33):49858–49869. https://doi.org/10.1007/s11356-022-19259-y

SERHAN M., SPROWLS M., JACKEMEYER D., LONG M., PEREZ I. D., MARET W., TAO N., FORZANI E. (2019) Total iron measurement in human serum with a smartphone. AIChE Annual Meeting, Conference Proceedings, 2019-November. https://doi.org/10.1039/x0xx00000x

SHETH Y., DHARASKAR S., KHALID M., SONAWANE S. (2021) An environment friendly approach for heavy metal removal from industrial wastewater using chitosan based biosorbent: A review. Sustainable Energy Technologies and Assessments, 43. https://doi.org/10.1016/j.seta.2020.100951

TB J., AA. A. (2010). Adsorption kinetics of cadmium and lead by chitosan. African Journal of Biotechnology, 9(17), 2560–2565. http://www.academicjournals.org/AJB

TiRTOM V. N., DINÇER A., BECERIK S., AYDEMIR T., ÇELIK A. (2012) Comparative adsorption of Ni(II) and Cd(II) ions on epichlorohydrin crosslinked chitosan-clay composite beads in aqueous solution. Chemical Engineering Journal, 197: 379–386. https://doi.org/10.1016/j.cej.2012.05.059

WITEK-KROWIAK A., CHOJNACKA K., PODSTAWCZYK D., DAWIEC A., POKOMEDA K. (2014) Application of response surface methodology and artificial neural network methods in modelling and optimization of biosorption process. Bioresource Technology, 160: 150–160. https://doi.org/10.1016/j.biortech.2014.01.021

XABA S. A., IGBERASE E., OSAYI J., SEODIGENG T., OSIFO P. O. (2020) Optimization of primary sewage sludge and coal lignite by microwave assisted pyrolysis for the production of bio oil. Environmental Technology (United Kingdom), 1–35. https://doi.org/10.1080/09593330.2020.1797903

ZHANG X., MA J., ZOU B., RAN L., ZHU L., ZHANG H., YE Z., ZHOU L. (2022) Synthesis of a novel bis Schiff base chelating resin for adsorption of heavy metal ions and catalytic reduction of 4-NP. Reactive and Functional Polymers, 180. https://doi.org/10.1016/j.reactfunctpolym.2022.105409